Journal of Superconductivity and Novel Magnetism (2021) 34:1341–1350
https://doi.org/10.1007/s10948-021-05862-6

ORIGINAL PAPER

Effects of Non-magnetic Metallic Zinc Nanoparticles on the Dielectric Properties of CuTl-1223 Superconducting Phase

Abrar A. Khan[1] · M. Mumtaz[1] · Mubasher[1] · M. Khan[1] · Liaqat Ali[1] · M. Rahim[1] · M. Ali[1]

Received: 12 February 2021 / Accepted: 11 March 2021 / Published online: 19 March 2021

Abstract

Synthesis of non-magnetic metallic zinc (Zn) nanoparticles (NPs) and $(Zn)_x/Cu_{0.5}Tl_{0.5}Ba_2Ca_2Cu_3O_{10-\delta}$ (CuTl-1223) nanoparticle-superconductor composites was carried out by chemical sol-gel and solid-state reaction methods, respectively. Different concentrations of Zn NPs from 1.0 to 4.0 wt.% were inserted in CuTl-1223 superconducting matrix to obtain desired $(Zn)_x$/CuTl-1223 nanoparticle-superconductor composites. The structural properties of these NPs and composites were studied by X-ray diffraction (XRD) technique. The unaffected crystal symmetry of the host CuTl-1223 superconducting phase after the inclusion of Zn NPs from XRD patterns suggested that these NPs were settled across the grain boundaries. Transport electrical properties of $(Zn)_x$/CuTl-1223 composites were investigated by resistivity versus temperature (RT) measurements, and zero resistivity critical temperature (T_c) was found to be increased with Zn NPs contents up to $x = 3$ wt.%. The enhancement in T_c could be due to the non-magnetic metallic Zn $3d^{10}$ ($S = 0$) NPs that facilitated the conduction of charge carriers across the grain boundaries, while T_c was suppressed beyond $x = 3$ wt.% contents of Zn NPs due to reduced superconducting volume fraction of CuTl-1223 matrix. Using the LCR meter, dielectric parameters, namely real part (ε'_r), imaginary part (ε''_r), tangent loss (tanδ), and ac-conductivity (σ_{ac}), were measured at varying frequencies and temperatures. The values of ε'_r, ε''_r and tanδ were found to be maximum at lower frequencies and became constant at high frequencies, while the value of σ_{ac} was found to be minimum at lower frequencies and was increased with increasing frequency.

Keywords CuTl-1223 superconducting phase · Non-magnetic metallic Zn nanoparticles · $(Zn)_x$/CuTl-1223 nanoparticle-superconductor composites · Transport electrical properties · Dielectric parameters

PASC Code 61.10.Nz · 75.47.Lx · 77.22.−d · 77.22.Ej

1 Introduction

Since the discovery of superconductivity, extensive researches on the materials, which show superconductive nature, have been carried out in order to acquire applications of superconductivity. This leads to the search of materials that show superconductive behavior at relatively high temperature than previously discovered mercury-based superconductors having superconductivity at low temperatures, i.e., 4 K. The search of high-temperature superconductors leads to the discovery of $(Cu_{1-x}Tl_x)Ba_2Ca_{n-1}Cu_nO_{2n-4-\delta}$, where $n = 2, 3, 4\ldots$, family, which showed superconductivity at temperatures as high as 135 K [1]. In order to improve the superconducting properties and find potential applications, these cuprates were researched extensively. $Cu_{0.5}Tl_{0.5}Ba_2Ca_2Cu_3O_{10-\delta}$ (CuTl-1223) is one of the prominent members of this family [2]. The properties of CuTI-1223 superconducting phase, which make it eminent, are its low superconducting anisotropy, high T_c (0) (zero resistivity critical temperature), high J_c (critical current density) and H_{irr} (high irreversibility field), long coherence length along the c-axis in their unit cell, and small penetration depth [3–6]. High-temperature superconductors (HTSCs) like CuTl-1223 can find potential applications in wide range of technological fields from electrical power industry to small electronic devices. In addition, the CuTI-1223 phase is easy to synthesize at ambient pressure [7–9]. Although the phase synthesized at high pressure

✉ M. Mumtaz
mmumtaz75@yahoo.com

[1] Materials Research Laboratory, Department of Physics, Faculty of Basic and Applied Sciences (FBAS), International Islamic University (IIU), H-10, Islamabad 44000, Pakistan

can give improved superconducting parameters, the synthesis on ambient pressure is more convenient. In electronic devices, the study of dielectric properties can give a thorough insight of the performance of a material as it can give information about charge mobility as well as charge storage in the form of polarization. The frequency, temperature, crystal defects, impurities, and synthesis conditions are responsible for the conduction and charge storage mechanism [10–15]. The presence of crystal defects such as inter-grain voids and grain boundaries hinder the charge mobility and are responsible for interfacial polarization, which contribute in the enhancement of dielectric properties. There are four different types of polarization that occur in a material when it is subjected to external ac field [16]. Each type of polarization becomes dominant at different frequency range; i.e., interfacial polarization has a dominant effect in frequency range between 10^3 Hz and few kHz, dipolar polarization in the range from 10^3 to 10^9 Hz, ionic polarization in 10^{10} to 10^{13} Hz, and electronic polarizations is usually observed at 10^{15} Hz frequency [17, 18]. For HTSCs, interfacial and dipolar polarizations are more prominently observed as they generally occur due to crystal defects. In order to find better and suitable use of HTSCs in technological applications, investigations of the dependence of their dielectric properties on frequency as well as temperature have huge significance. On the other hand, a great deal of attention is also focused on mitigation of the factors that hinders the performance of HTSCs like crystal defects using different techniques by improving synthesis processes or addition of nanomaterials on grain boundaries.

Superconducting as well as frequency-dependent dielectric properties of $BaFe_{12}O_{19}$ added (Bi,Pb)-2223 superconductor was studied with varying operating temperatures from 77 to 296 K. The dielectric parameters showed strong dependence on the operating temperature as these parameters decreased with increasing temperature [19]. MgO was added in $Cu_{0.25}Tl_{0.7}5Ba_2Ca_3Cu_4O_{12-\delta}$ superconductor in order to heal the micro-cracks and improve inter-grain connectivity. The dielectric study revealed that ac-conductivity was suppressed, while ε'_r showed enhancement with increasing MgO concentrations [20]. The dielectric properties of CuTl-1223 superconducting phase were studied at varying frequencies and temperatures with the addition of different concentrations of ZnO nanoparticles. The addition of ZnO nanoparticles improved the inter-grain connectivity by stuffing of the voids present in the grains. The dielectric properties of these composites showed usual direct relation with frequency, whereas they showed inverse relation with temperatures [21]. The dielectric properties of CuTl-1234 superconducting phase with the doping of Zn showed a decreasing trend with increasing frequency except the real part of dielectric constant [22]. Dielectric properties of silver added CuTl-1223 were studied in the frequency range of 40 Hz to 100 MHz between 77 and 253 K. The increment in silver contents in CuTl-1223 matrix up to 2.0 wt.% suppressed the values of dielectric constants, but with further increase in silver nanoparticles enhanced the dielectric constants. Ac-conductivity showed an opposite behavior as compared to dielectric constants owing to the settlement of silver nanoparticles on the grain boundaries due to the contribution in the space charge polarization [7, 23, 24]. The dielectric properties as well as complex impedance spectroscopy of $YBa_2Cu_3O_{7-\delta}$ (Y-123) superconductors were studied with the addition of $HoMnO_3$. The study suggested that the real and imaginary part of dielectric constant was increased with increased $HoMnO_3$ contents in Y-123 superconductor [25]. From the past investigations, it is established that charge stockpiling and ac-conduction process in HTSCs relied on temperature, frequency, surface charges, fabrication process, and doping contents of the material [8, 15, 19, 26].

The non-magnetic metallic zinc {Zn $3d^{10}$ ($S = 0$)} nanoparticles have been added at the grain boundaries of CuTl-1223 superconducting phase. The main objective was to reduce the magnetic interaction and scattering of carriers causing Cooper pair-breaking taking place across the grain boundaries during the transition from a normal state to a superconducting state. So the superconducting properties were expected to be enhanced with the addition of these nanoparticles. Secondly, the normal state resistivity was also expected to be reduced after the addition of these non-magnetic Zn nanoparticles due to reduced magnetic interaction with normal electrons. In this study, the novelty was to explore the effect of non-magnetic metallic Zn $3d^{10}$ ($S = 0$) nanoparticles addition across the grain boundaries on the ac-conduction properties of CuTl-1223 superconducting phase via dielectric measurements. This study can further give insight about the effects of these nanoparticle additions on the superconducting properties of cuprate superconductors.

2 Experimental

2.1 Preparation of Zn Nanoparticles

The Zn nanoparticles were prepared by sol-gel method, and the synthesis process was started by preparing two solutions. To make the first solution, appropriate quantities of Zn nitrate and ethanol were mixed with each other. The second solution was obtained by adding citric acid in distilled water, and this solution was added drop-wise into the first solution. To regulate the pH of the solution, ammonia was added drop-wise. Furthermore, the gel was formed with continuous stirring at 85 °C. The gel was then placed in a microwave oven for drying at 100 °C for 12 h. The dried material was ground in agate mortar and pestle. The ground material was annealed in furnace for 2 h at 600 °C. Finally, the nanoparticles were obtained after grinding the annealed material.

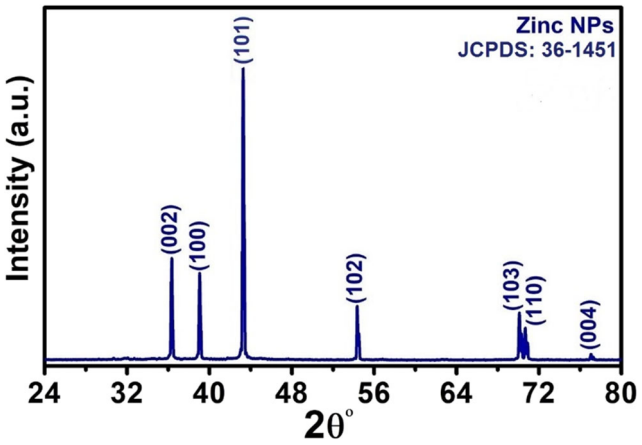

Fig. 1 X-ray diffraction pattern of metallic Zn nanoparticles

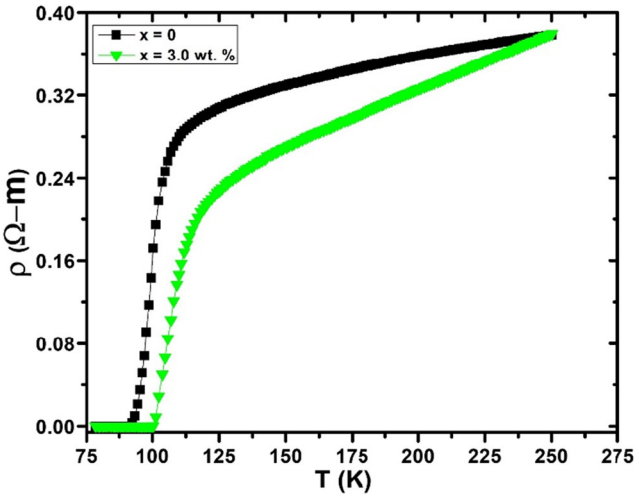

Fig. 3 Resistance vs. temperature graphs of representative $(Zn)_x$/CuTl-1223; x = 0, and 3 wt.% nanoparticle-superconductor composites

2.2 Preparation of $(Zn)_x$/CuTl-1223 Nanoparticle-Superconductor Composites

The CuTl-1223 phase was synthesized by the solid-state reaction method. Initially, the nitrates of Cu $(CN)_2$, Ca $(NO_3)_2$, and Ba $(NO_3)_2$ were taken with stoichiometric ratios and mixed with each other by grinding using an agate mortar and pestle for 2 h. After grinding, the sample was placed in furnace for heating at 860 °C for 24 h. The furnace was then cooled to room temperature, and the sample was again ground for 2 h followed by heat treatment for 24 h. Tl_2O_3 and Zn nanoparticles were added in the precursor and again ground for 1 h. The mixed and ground material was then pressed in the form of the disc and wrapped in gold capsules. These pellets enclosed in gold capsules were sintered in pre-heated furnace at 860 °C for 10 min to obtain $(Zn)_x$/CuTl-1223; $x = 0$, 1, 2, 3 and 4 wt.% nanoparticle-superconductor composites.

3 Results and Discussion

X-ray diffraction (XRD) was performed to confirm the phase formation and crystallographic structure of $(Zn)_x$/CuTl-1223 nanoparticle-superconductor composites. XRD peaks of Zn nanoparticles corresponding Bragg's angles at 2θ = 36.34°, 39.06°, 43.28°, 54.36°, 70.1°, 70.68°, and 77.04° were properly indexed to (002), (100), (101), (102), (103), (110), and (004) planes respectively, as shown in Fig. 1. The crystalline structure of Zn nanoparticles was validated by a JCPDS card, which confirmed that metallic Zn nanoparticles are of hexagonal structure. None of the notable peaks other than the peaks of Zn nanoparticles was observed. Debye Scherer's formula was employed to calculate the average crystallite size of these metallic Zn nanoparticles that were found approximately 50 nm. XRD patterns of

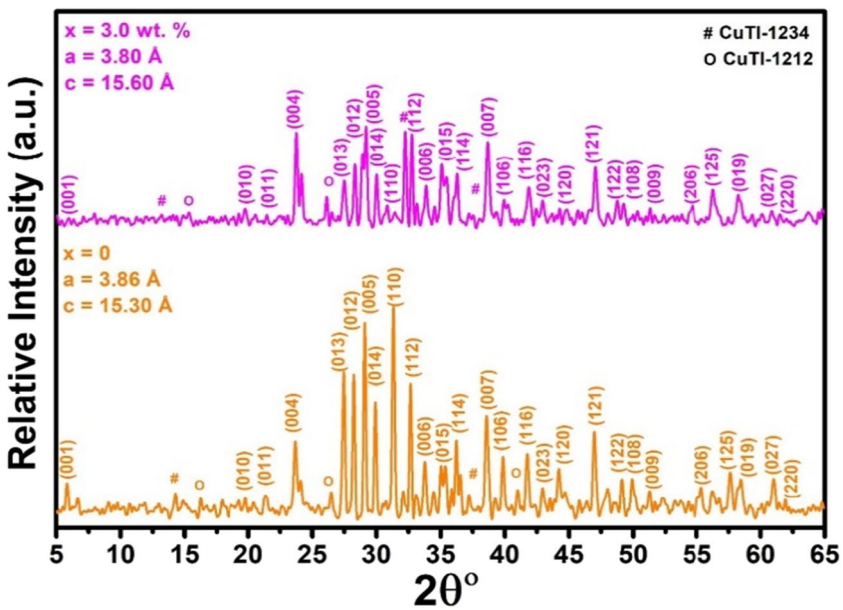

Fig. 2 X-ray patterns of representative $(Zn)_x$/CuTl-1223; x = 0, and 3 wt.% nanoparticle-superconductor composites

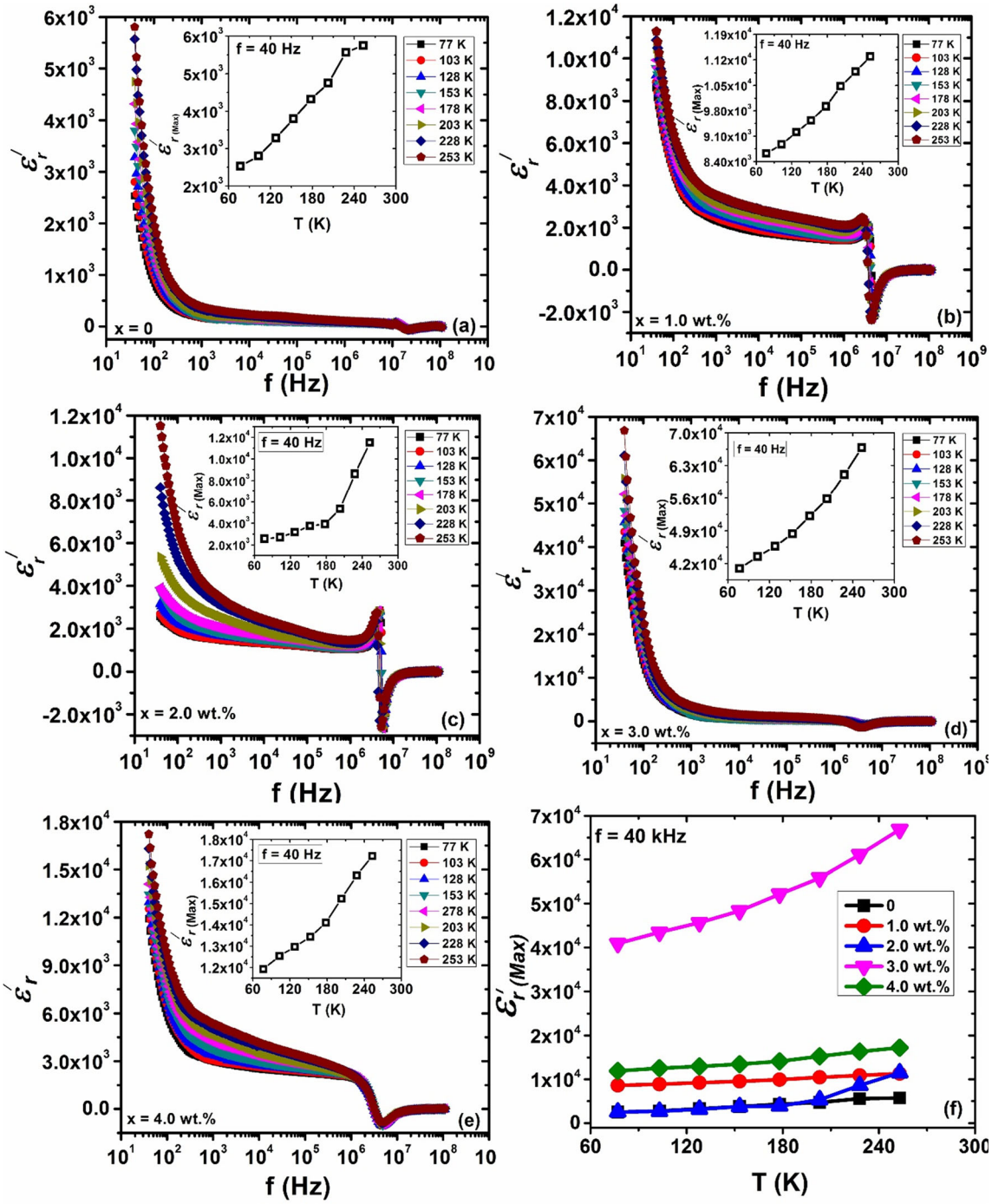

Fig. 4 **a**–**e** Real part as function of frequency at various temperatures of $(Zn)_x$/CuTl-1223; x = 0, 1, 2, 3, and 4 wt.% nanoparticle-superconductor composites. **f** Variation of real part with various temperatures at 40 Hz

representative $(Zn)_x$/CuTl-1223; x = 0, and 3 wt.% nanoparticle-superconductor composites are given in Fig. 2. The XRD results exhibited that metallic Zn nanoparticles did not affect the tetragonal structure of CuTl-1223 matrix, which means that metallic Zn nanoparticles reside at the grain boundaries. In XRD spectra of $(Zn)_x$/CuTl-1223 composites, the unknown peaks of low intensities were also observed which could be associated to impurities and other superconducting phases.

RT measurements of representative $(Zn)_x$/CuTl-1223; x = 0, and 3 wt.% nanoparticle-superconductor composites are shown in Fig. 3. The improvement in superconducting properties can be associated to less scattering and Cooper pair-breaking across the grain boundaries after metallic Zn nanoparticles due to their non-magnetic nature. Secondly, the inter-grain weak links were improved by filling the voids and pores with Zn nanoparticles. In this way, the required

Table 1 Variation in maximum values of dielectric parameters of $(Zn)_x$/CuTl-12231223; x = 0, 1, 2, 3, and 4 wt.% nanoparticle-superconductor composites with varying concentrations of Zn nanoparticles from 77 to 253 K

Dielectric parameters	Contents (wt.%)	Temperature (K)							
		77	103	128	153	178	203	228	253
ε'_r	0	2529.1	2800.0	3279.7	3798.8	4318.8	4749.0	5568.9	5748.1
	1	8622.9	8880.5	9214.1	9539.0	9925.3	10,475.5	10,879.4	11,289.1
	2	2565.6	2703.1	3172.9	3772.6	3916.8	5352.8	8629.0	11,512.4
	3	40,913.6	43,483.2	45,665	48,366.02	52,169.0	55,848.0	61,111.6	66,857.5
	4	11,927.1	12,544.2	12,969.1	13,443.1	14,109.4	15,236.4	16,318.6	17,226.7
ε''_r	0	3.45×10^7	3.46×10^7	3.47×10^7	3.47×10^7	3.48×10^7	3.50×10^7	3.52×10^7	3.55×10^7
	1	1.88×10^7	1.9×10^7	1.92×10^7	1.94×10^7	1.98×10^7	2.04×10^7	2.12×10^7	2.20×10^7
	2	3.34×10^6	3.46×10^6	3.65×10^6	3.82×10^6	4.03×10^6	4.15×10^6	4.28×10^6	4.34×10^6
	3	1.01×10^8	1.01×10^8	1.03×10^8	1.05×10^8	1.07×10^8	1.13×10^8	1.21×10^8	1.29×10^8
	4	1.71×10^7	1.72×10^7	1.73×10^7	1.75×10^7	1.78×10^7	1.80×10^7	1.84×10^7	1.88×10^7
tanδ	0	6615.40	6486.80	6413.08	6227.93	6134.68	6079.97	5978.71	5865.20
	1	2816.94	2653.34	2457.72	2403.75	2373.95	2305.93	2238.47	2164.27
	2	1139.50	1059.05	1006.88	890.58	819.05	799.25	726.88	666.50
	3	28,957.76	28,137.42	26,912.50	25,822.79	25,550.46	23,339.90	21,319.90	18,904.02
	4	2135.60	2032.33	1945.16	1864.69	1774.83	1607.23	1550.32	1409.11
σ_{ac}	0	0.000653	0.000657	0.00066	0.000669	0.000679	0.000689	0.000701	0.000720
	1	0.00651	0.00659	0.00660	0.00671	0.00679	0.00682	0.00692	0.00702
	2	0.00770	0.00782	0.00792	0.00800	0.00802	0.00808	0.00817	0.00825
	3	0.00249	0.00253	0.00255	0.00257	0.00259	0.00260	0.00267	0.00275
	4	0.00837	0.00861	0.00877	0.00885	0.00899	0.00916	0.00932	0.00954

carriers' concentration for desired superconductivity can be achieved.

The dielectric study of $(Zn)_x$/CuTl-1223; x = 0, 1, 2, 3, and 4 wt.% composites was performed at 77 to 253 K temperatures in 40 Hz to 100 MHz frequency range. Koop's theory and Maxwell-Wagner model have been used to explain the variations in dielectric properties with respect to applied frequency. According to these theories, polycrystalline materials are composed of grains and grain boundaries. The electrical nature of the grains is conducting, while the grain boundaries act as semi/non-conducting medium for electrical charge carriers. On the application of external electric field, charges or electrons travel via hopping process from the grains to the grain boundaries [27, 28]. When the material is subjected to electric field, it gets polarized and stores the energy in the form of polarization. The energy retained in the material is represented by the real part of dielectric constant and denoted by ε'_r. Figure 4 a–e shows the plot between ε'_r and frequency f(Hz) at different temperatures (T) in the range from 77 to 253 K for $(Zn)_x$/CuTl-1223; x = 0, 1, 2, 3, and 4 wt.% composites. Maximum values of ε'_r were found at the low frequency (i.e.; 40 Hz) owing to the presence of all types of the polarizations. It is obvious from Fig. 4 a–e that ε'_r showed a declining trend with increasing frequency, which is due to smaller relaxation time at higher frequency. Moreover, due to small relaxation time, charges present in the material could not follow the rapid change in the direction of applied ac field [29]. The value of ε'_r was increased with addition of metallic Zn nanoparticles in CuTl-1223 superconducting phase up to x = 3 wt.%. The preliminary enhancement in ε'_r can be linked to the settlement of Zn nanoparticles across the grain boundaries and improved the interface area that resulted in the increased polarization. In addition, further increase in the concentration of Zn nanoparticles can cause agglomeration and segregation in certain regions of the grain boundary, which can reduce the degree of polarization in the material. Thus, the decreasing polarization can reduce the capacitance values, and as a result, ε'_r is decreased. The variation in ε'_r as a function of temperature is shown in Fig. 4 f and Table 1. With rise in temperature, ε'_r is increased as the grains and grain boundaries have been expanded at high temperatures, whereas charge carriers got more energy to reach grain boundaries and take part in interfacial polarization [29, 30].

Energy is stored in the form of polarization when a material is placed in an external electric field, but some of the charges present in the material begin flowing in the directions of the applied field; these charges contribute in the energy losses. These energy losses are related to the imaginary part of

dielectric constant and denoted by ε''_r. Figure 5 a–e shows the variation of ε''_r in a frequency range from 40 Hz to 100 MHz at different temperatures from 77 to 253 K for $(Zn)_x$/CuTl-1223; $x = 0$, 1, 2, 3, and 4 wt.% composites. At low frequency, ε''_r values are higher because charge carriers are given additional time to pass through the conducting grains at low frequency. But at higher frequencies, the motion of charge carriers was hindered by the charge carriers that resulted in the decrease in ε''_r. The dipoles change their direction with the change of direction of the applied field, and the dipoles lose their energy during their alignment, which also contributes in energy losses. However, the time constant of the applied electrical field drops significantly with rising frequency; this makes it difficult to align dipoles properly in a very short time. So, the motion of dipoles was also limited at high frequency, which resulted in less energy losses and as a result ε''_r became saturated at very high frequency. The values of ε''_r was increased by introducing metallic Zn nanoparticles in CuTl-1223 superconducting matrix as shown in Fig. 5 a–f. The connectivity between grains and grain boundaries was

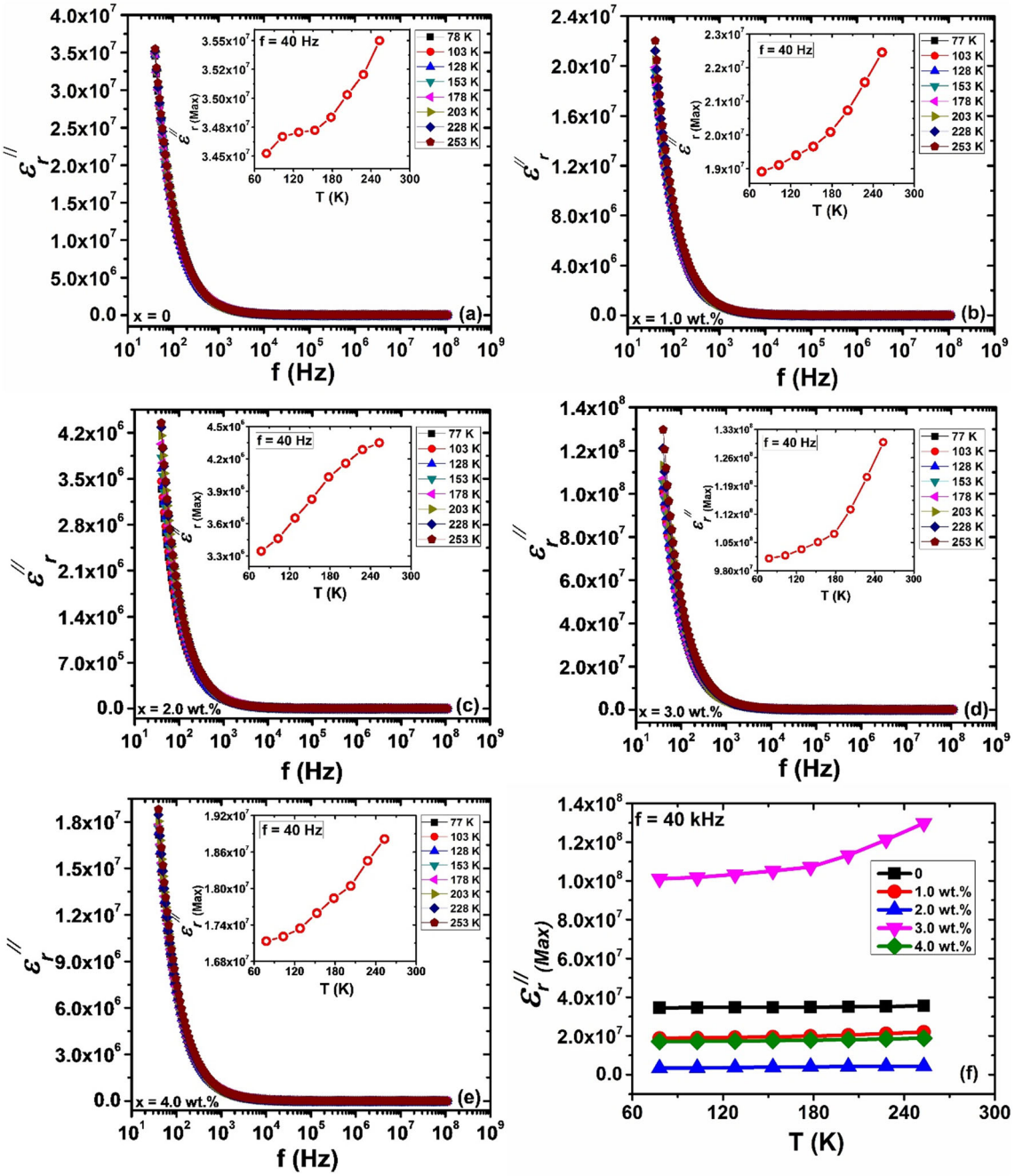

Fig. 5 **a–e** Imaginary part as function of frequency at various temperatures of $(Zn)_x$/CuTl-1223; $x = 0$, 1, 2, 3, and 4 wt.% nanoparticle-superconductor composites. **f** Variation of imaginary part with various temperatures at 40 Hz

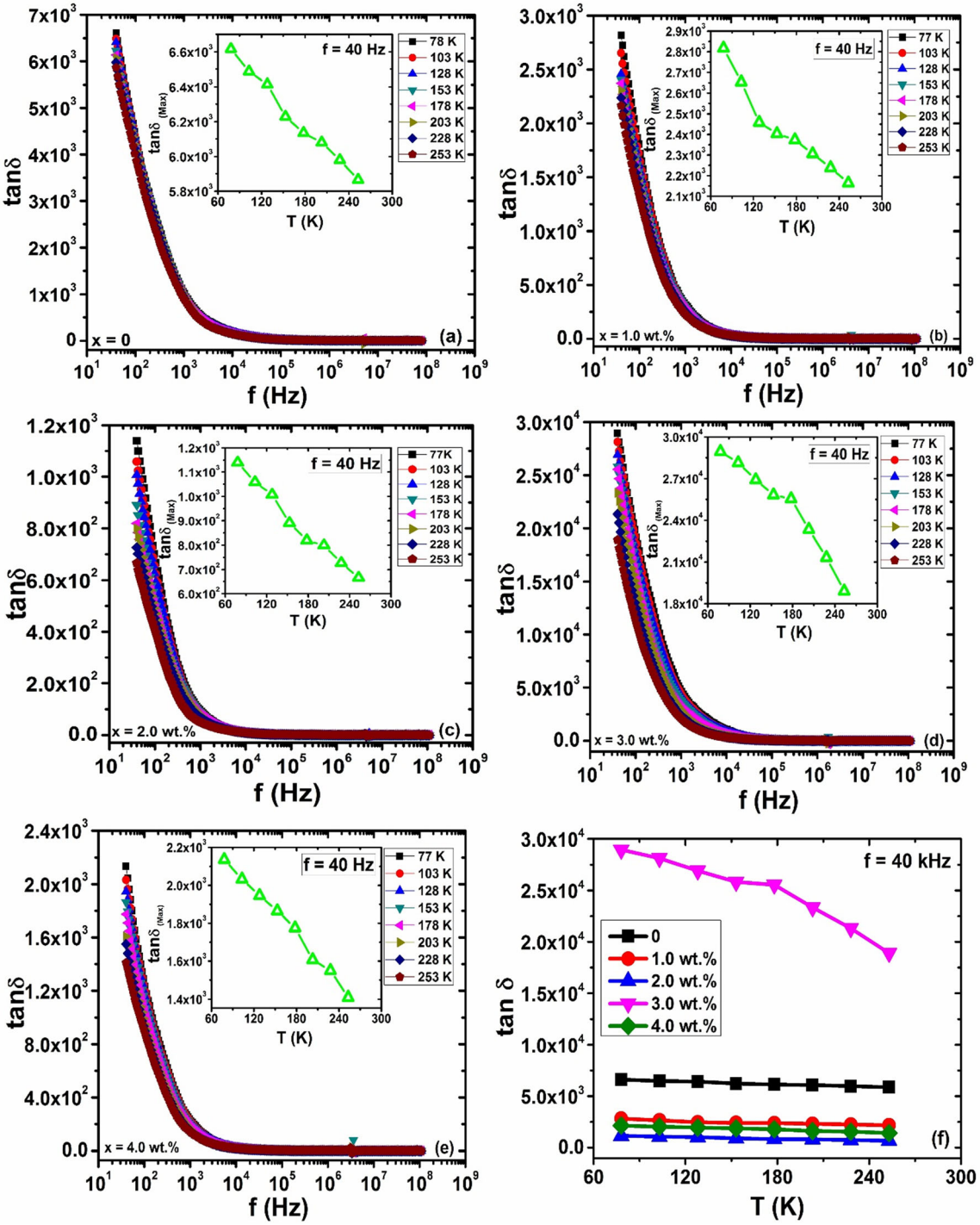

Fig. 6 **a–e** Tangent loss as function of frequency at various temperature of $(Zn)_x$/CuTl-1223; x = 0, 1, 2, 3, and 4 wt.% nanoparticle-superconductor composites. **f** Variation of tangent loss with various temperatures at 40 Hz

enhanced due to the stuffing of metallic Zn nanoparticles on grain boundaries. The effect of temperature on ε''_r is shown in Fig. 5 f and Table 1. The values of ε''_r were increased with increasing temperature because at high temperatures, the dipoles, ions, and atoms vibrate with high amplitude and collide with each other more frequently. As a result, energy losses increase which give higher values of ε''_r [31].

Tangent loss (tanδ) is the fractional loss calculated by ratio of ε''_r and ε'_r of dielectric constant. Figure 6 a–f displays the variation in tanδ with respect to frequency and temperature for $(Zn)_x$/CuTl-1223; x = 0, 1, 2, 3, and 4 wt.% composites. As tanδ is the fractional loss obtained from the ratio of ε''_r to ε'_r, so it showed almost the same trend as ε'_r and ε''_r with respect to frequency. At low frequency, the values of tanδ are maximum due to high

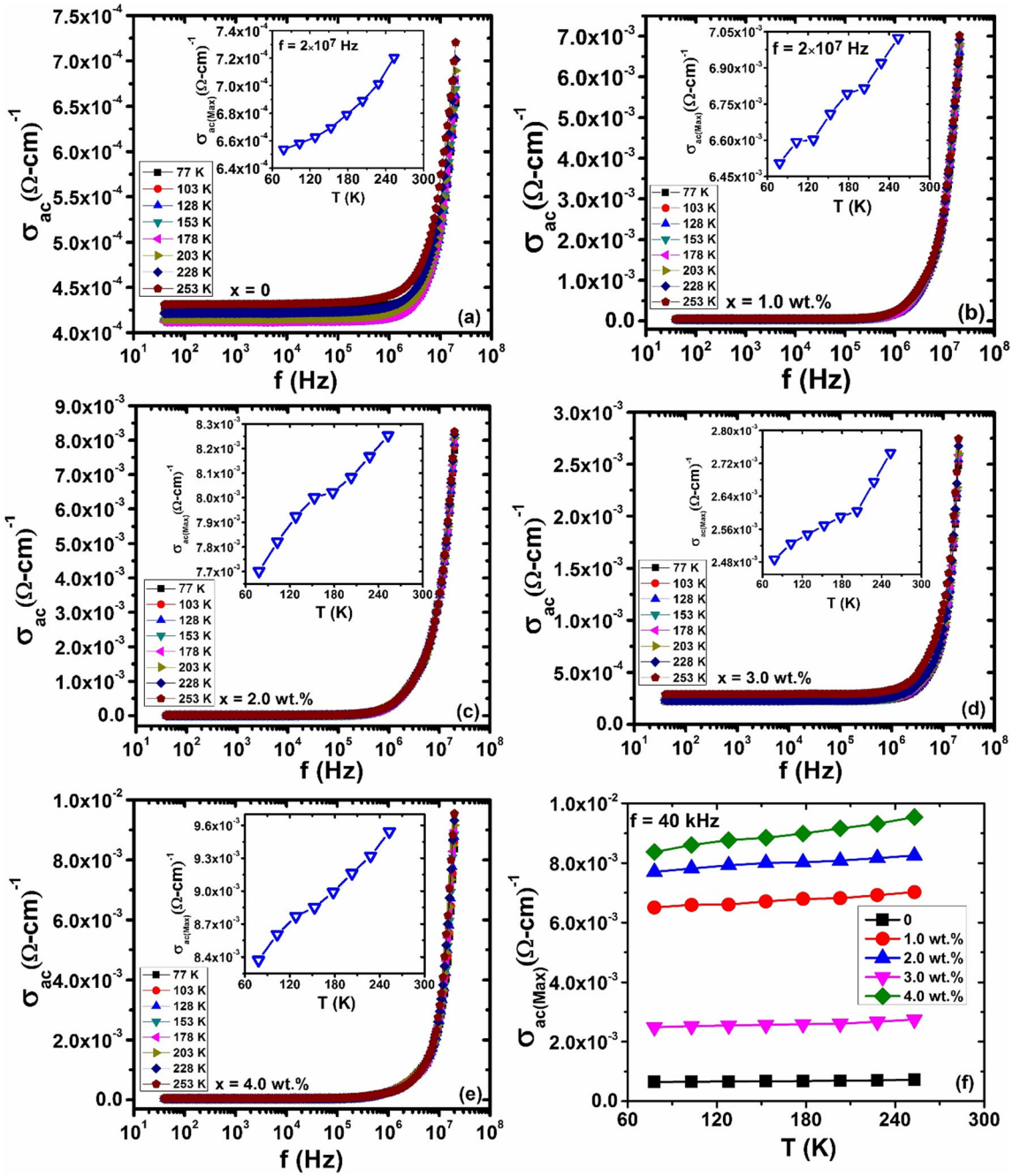

Fig. 7 **a–e** Ac-conductivity as function of frequency at various temperature of $(Zn)_x$/CuTl-1223; $x = 0$, 1, 2, 3, and 4 wt.% nanoparticle-superconductor composites. **f** Variation of ac-conductivity with various temperatures at 40 Hz

relaxation time, which results in the movement of charges in the direction of ac field. In addition, frequent change in the direction of dipoles of material leads to loss of energy in the form of heat; thus, the more the charges move, the more they contribute in losses. Furthermore, the decrease in the relaxation time of applied electric field occurred with increasing frequency and due to low relaxation time at high frequency, dipoles' and charges' movements decreased and almost ceased at the end as they cannot follow the applied field. So, at high frequency, tanδ decreases and became constant due to the small movement of charges. Fig. 6 a–f indicates that when the content of Zn nanoparticles was increased in the given superconducting matrix, tanδ initially decreased up to a certain value and then started to increase. The increase in concentration of Zn nanoparticles increased the polarization at interfaces as the Zn nanoparticles did not enter the grains and set on grain boundaries; as a result, the charge storage was enhanced, which led to decrease in tanδ. Furthermore, the increase in concentration of Zn nanoparticles can increase agglomerations and segregations, which led to higher losses, and hence, tanδ was decreased. The variation in

values of tanδ with temperatures is shown in Fig. 6 f and Table 1. The increase in the values of tanδ with temperatures may be due to the increase in thermal energy acquired by the charges with increasing temperature, which led to an increase in their motion. An increase in motion of charge resulted in more losses, so tanδ increases with increasing temperature [32].

When the electric field is applied to a dielectric material, charges start to be stored in the form of polarization, but some charge carriers starts to flow in the direction of field. The ac-conductivity is the measurement of the flowing charges, and it is denoted by σ_{ac}. Figure 7 a–f displays the variation of σ_{ac} with respect to frequency and temperature for $(Zn)_x$/CuTl-1223; x = 0, 1, 2, 3, and 4 wt.% composites. Figure 7 a–f illustrates that the values of σ_{ac} were enhanced with increasing values of frequencies and temperature. According to Koops' theory and Maxwell-Wagner's model, conducting grains become active at high frequency, so σ_{ac} shows enhancement with increasing frequency. In addition, the decrease in relaxation time of the applied electric field at high frequency prevents charge carriers to get polarized so they take part in enhancement of σ_{ac} [33]. The increasing contents of Zn nanoparticles in CuTl-1223 superconducting phase enhanced the values of σ_{ac}, which can be referred to the better inter-grain connectivity that sported the charge carriers to flow through the material. The variation of σ_{ac} with temperature at frequency of 40 Hz is given in Table 1 and Fig. 7 f. On increasing temperature, more number of charge carriers get energy to flow, and as a result, the rate of movement of the charge carriers' increases [34, 35]. Therefore, the values of σ_{ac} for $(Zn)_x$/CuTl-1223 nanoparticle-superconductor composites were increased with increasing temperatures.

4 Conclusion

Sol-gel method and solid-state reaction methods were employed for the synthesis of Zn NPs and $(Zn)_x$/CuTl-1223 nanoparticle-superconductor composites, respectively. XRD confirmed the settlement of Zn NPs across the grain boundaries as no significant change occurred in the XRD spectra of CuTl-1223 phase with the inclusion of Zn NPs. RT plots indicated the increase in T_c (0) by stuffing the voids and pores with the addition of Zn NPs. The dielectric parameters (ε'_r and ε''_r) were found maximum at low frequency owing to larger relaxation time of the frequency of the ac field. The decreasing trend became the smallest at high frequency due to very low relaxation time provided by the applied ac field, which was almost impossible to be followed by the charge carriers. The σ_{ac} shows increasing trend with increasing frequency owing to more active grains at high frequency. The enhancement in ε'_r and ε''_r with decreasing temperature and increase in σ_{ac} at higher temperature can be attributed to better availability and chances of charge carriers to flow at high temperatures because of the acquisition of thermal energy.

References

1. Shrivastava, S.K.: Search for higher critical temperature (T_c) in superconducting materials. Int. J. Eng. Sci. Res. **5**, 40–54 (2017)
2. Yamamoto, H., Tanaka, K., Tokiwa, K., Hirabayashi, H., Tokumoto, M., Khan, N.A., Ihara, H.: Synthesis of $Cu_{1-x}Tl_xBa_2Ca_2Cu_3O_{11-y}$ (x~0.7) superconductor by hot press. Physica C. **302**, 137–142 (1998)
3. Awad, R.: Enhancement the formation of (Cu, Tl)-1223 superconducting phase by Cd-substitution. J. Alloys Comp. **474**, 517–521 (2009)
4. Ihara, H., Tanaka, K., Tanaka, Y., Iyo, A., Terada, N., Tokumoto, M., Ariyama, M., Hase, I., Sundaresan, A., Hamada, N., Miyashita, S., Tokiwa, K., Watanabe, T.: Mechanism of T_c enhancement in $Cu_{1-x}Tl_x$-1234 and -1223 system with T_c>130 K. Physica C. **341–348**, 487–488 (2000)
5. Ihara, H.: How to achieve the best performance superconductor based on Cu-1234. Physica C. **364–365**, 289–297 (2001)
6. Tanaka, K., Iyo, A., Terada, N., Tokiwa, K., Miyashita, S., Tanaka, Y., Tsukamoto, T., Agarwal, S.K., Watanabe, T., Ihara, H.: Tl valence change and T c enhancement (> 130 K) in (Cu, Tl)$Ba_2Ca_2Cu_3O_y$ due to nitrogen annealing. Phys. Rev. B. **63**, 064508 (2001)
7. Khan, A.A., Sohail, M., Rahim, M., Mumtaz, M., Khan, M.N.: Frequency and temperature dependent dielectric constant of $(Ag)_x$/CuTl-1223 nanoparticles-superconductor composites. J. Alloys Compd. **825**, 154138 (2020)
8. Kalsi, S.S.: Applications of high temperature superconductors to electric power equipment. Wiley, Hoboken (2011)
9. Hull, J.R.: Applications of high-temperature superconductors in power technology. Rep. Prog. Phys. **66**, 1865 (2003)
10. Li, L., Richter, C., Paetel, S., Kopp, T., Mannhart, J., Ashoori, R.C.: Very large capacitance enhancement in a two-dimensional electron system. Science. **332**, 825 (2011)
11. Hench, L.L., West, J.K.: Principles of electronic ceramics. Wiley, New York (1990)
12. Koseoglu, Y., Kurtulus, F., Kockar, H., Guler, H., Karaagac, O., Kazan, S., Aktas, B.: Magnetic characterizations of cobalt oxide nanoparticles. J. Supercond. Nov. Magn. **25**, 2783–2787 (2012)
13. Karaagac, O., Kockar, H.: Iron oxide nanoparticles co-precipitated in air environment: effect of $[Fe^{+2}]/[Fe^{+3}]$ ratio. IEEE Trans. Magn. **48**, 1532–1536 (2012)
14. Ozel, F., Kockar, H., Beyaz, S., Karaagac, O., Tanrisever, T.: Superparamagnetic iron oxide nanoparticles: effect of iron oleate precursors obtained with a simple way. J. Mater. Sci. Mater. Electron. **24**(8), 3073–3080 (2013)
15. Karaagac, O., Bilir, B., Kockar, H.: Superparamagnetic cobalt ferrite nanoparticles: effect of temperature and base concentration. J. Supercond. Nov. Magn. **28**, 1021–1027 (2015)
16. Şafak-Asar, Y., Asar, T., Altındal, Ş., Özçelik, S.: Investigation of dielectric relaxation and ac electrical conductivity using impedance spectroscopy method in (AuZn)/TiO_2/p-GaAs (110) schottky barrier diodes. J. Alloys Compd. **628**, 442–449 (2015)
17. Ben-Ishai, P., Sader, E., Feldman, Y., Felner, I., Wegar, M.: Dielectric properties of $Na_{0.7}CoO_2$ and of the superconducting $Na_{0.3}CoO_{2\cdot1}.3H_2O$. J. Supercond. **18**, 455–459 (2005)
18. Annabi, M., Bouchoucha, I., Azzouz, F.B., Salem, M.B.: Effect of ZnO and $Zn_{0.95}Mn_{0.05}O$ nano-particle inclusions on YBCO

polycrystalline pinning properties. IOP Conf. Ser.: Mater. Sci. Eng. **13**, 012009 (2010)
19. Khulud, H., El Haj Hassan, F., Awad, R.: Physical and dielectric properties of (Bi,Pb)-2223 superconducting samples added with $BaFe_{12}O_{19}$ nanoparticles. Chem Phys Lett. **757**, 13788016 (2020)
20. Mohammed, N.H.: Effect of MgO nano-oxide additions on the superconductivity and dielectric properties of $Cu_{0.25}Tl_{0.}75Ba_2Ca_3Cu_4O_{12-\delta}$ superconducting phase. J. Supercond. Nov. Magn. **25**, 45–53 (2012)
21. Mumtaz, M., Ali, L., Jabbar, A., Rabbani, M.W., Naveed, M., Imran, M., Amin, B., Khan, M.N., Sajjid, M.U.: Tuning of dielectric properties of $(ZnO)_x$/(CuTl-1223) nanoparticles superconductor composites. Ceram. Int. **42**, 11193 (2016)
22. Younis, A., Khan, N.A., Bajwa, N.U.: Dielectric properties of $Cu_{0.5}Tl_{0.5}Ba_2Ca_3Cu_{4-y}Zn_yO_{12-d}$ (y = 0, 3) superconductors. J. Korean Phys. Soc. **57**, 1437–1443 (2010)
23. Karaagac, O., Kockar, H.: A simple way to obtain high saturation magnetization for superparamagnetic iron oxide nanoparticles synthesized in air atmosphere: Optimization by experimental design. J. Magn. Magn. Mater. **409**, 116–123 (2016)
24. Karaagac, O., Yildiz, B.B., Köçkar, H.: The influence of synthesis parameters on one-step synthesized superparamagnetic cobalt ferrite nanoparticles with high saturation magnetization. J. Magn. Magn. Mater. **473**, 262–267 (2019)
25. Bahboh, A., Shaari, A.H., Baqiah, H., Kien, C.S., Kechik, M.M.A., Wahid, M.H., Talib, Z.A.: Effects of $HoMnO_3$ nanoparticles addition on microstructural, superconducting and dielectric properties of $YBa_2Cu_3O_{7-\delta}$. Ceram. Int. **45**, 13732–13739 (2019)
26. Cavdar, S., Koralay, H., Tugluoglu, N., Gunen, A.: Frequency-dependent dielectric characteristics of Tl–Ba–Ca–Cu–O bulk superconductor. Supercond. Sci. Technol. **18**, 1204 (2005)
27. Wagner, K.W.: The theory of heterogenous dielectric. Ann. Phys. **345**, 817 (1983)
28. Chen, J.W., Wang, J.C., Chen, Y.F.: Study of dielectric relaxation behavior in Nd_2CuO_4. Physica C. **289**, 131 (1997)
29. Vinila, V.S., Isac, J.: Temperature and frequency dependence of dielectric properties of superconducting ceramic $GdBa_2Ca_3Cu_4O_{10.5}$. Int. J. Sci. Res. **7**, 696–702 (2018)
30. Konopka, J., Jose, R., Wolcyrz, M.: Dielectric properties of ferromagnetic Ni nanoparticles added $(Cu_{0.5}Tl_{0.5})Ba_2Ca_2Cu_3O_{10-d}$ superconducting phase. Physica C. **435**, 53 (2006)
31. Rey, C.M., Mathias, H., Testardi, L.R., Skirius, S.: High dielectric constant and nonlinear electric response in nonmetallic $YBa_2Cu_3O_{6+\delta}$. Phys. Rev. B. **45**, 10639 (1992)
32. Çavdar, S., Koralay, H., Altındal, S.: Effect of vanadium substitution on the dielectric properties of glass ceramic Bi-2212 superconductor. J. Low Temp. Phys. **164**, 102 (2011)
33. Elliott, S.R.: Ac conduction in amorphous chalcogenide and pnictide semiconductors. Adv. Phys. **36**, 135–217 (1987)
34. Cohen, R.E.: Theory of ferroelectric: a vision for next decade and beyond. J. Phys. Chem. Solids. **61**, 139 (2000)
35. Mumtaz, M., Ali, L.: Mubasher, A. Saleh, Y. Slimani, I. Qasim, M. Hassan, and Z. Ahmad, "AC conduction mechanism via dielectric measurements of $(Cr)_x$/(CuTl)-1223 nanoparticles-superconductor composites". Cryogenics. **105**, 103021 (2020)